



HAL
open science

Molecular Engineering of Electrocatalytic Nanomaterials for Hydrogen Evolution: The Impact of Structural and Electronic Modifications of Anchoring Linkers on Electrocatalysis

Andrew Joshua Bagnall, Matthieu Haake, Sergi Grau, Tatiana Straistari, Matthieu Koepf, Navid Jameei Moghaddam, Carolina Gimbert-Suriñach, Jordi Benet-Buchholz, Antoni Llobet, Murielle Chavarot-Kerlidou, et al.

► To cite this version:

Andrew Joshua Bagnall, Matthieu Haake, Sergi Grau, Tatiana Straistari, Matthieu Koepf, et al.. Molecular Engineering of Electrocatalytic Nanomaterials for Hydrogen Evolution: The Impact of Structural and Electronic Modifications of Anchoring Linkers on Electrocatalysis. ACS Catalysis, 2024, 14, pp.5630-5638. 10.1021/acscatal.4c00336 . hal-04537292

HAL Id: hal-04537292

<https://hal.science/hal-04537292v1>

Submitted on 23 Oct 2024

HAL is a multi-disciplinary open access archive for the deposit and dissemination of scientific research documents, whether they are published or not. The documents may come from teaching and research institutions in France or abroad, or from public or private research centers.

L'archive ouverte pluridisciplinaire **HAL**, est destinée au dépôt et à la diffusion de documents scientifiques de niveau recherche, publiés ou non, émanant des établissements d'enseignement et de recherche français ou étrangers, des laboratoires publics ou privés.

Molecular engineering of electrocatalytic nanomaterials for hydrogen evolution: the impact of structural and electronic modifications of anchoring linkers on electrocatalysis.

Andrew J. Bagnall,^{‡,1,2,3} Matthieu Haake,^{‡,1} Sergi Grau,⁴ Tatiana Straistari,¹ Matthieu Koepf,¹ Navid Jameei Moghaddam,⁴ Carolina Gimbert-Suriñach,^{4,5} Jordi Benet-Buchholz,⁴ Antoni Llobet,^{4,5} Murielle Chavarot-Kerlidou,¹ Bertrand Reuillard,¹ and Vincent Artero^{1,}*

¹Univ. Grenoble Alpes, CNRS, CEA, IRIG, Laboratoire de Chimie et Biologie des Métaux, 17 rue des Martyrs, F-38054 Grenoble, Cedex, France.

²Ångström Laboratory, Department of Chemistry, Uppsala University, SE75120 Uppsala, Sweden.

³Université de Pau et des Pays de l'Adour, E2S UPPA, CNRS, IPREM UMR 5254, Pau 64012, France.

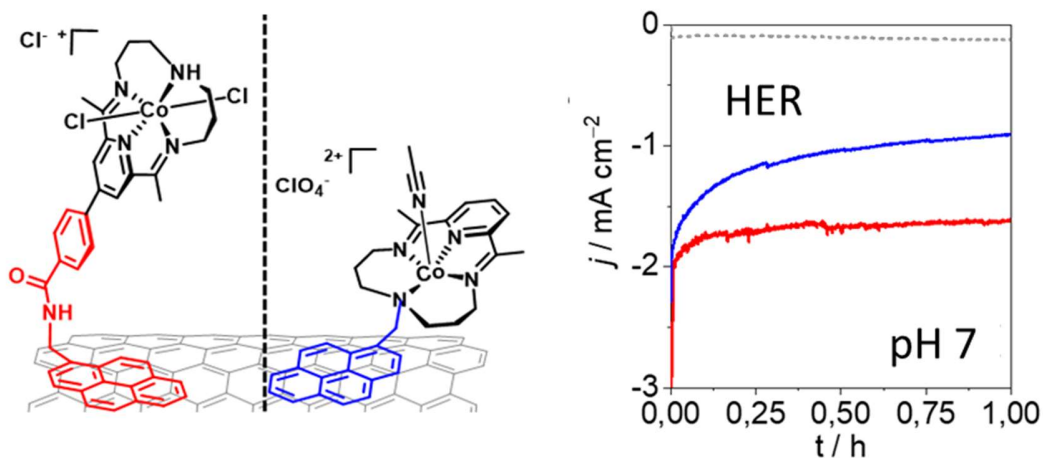
⁴Institute of Chemical Research of Catalonia (ICIQ), Barcelona Institute of Science and Technology (BIST), Avda. Països Catalans 16, 43007 Tarragona, Spain.

⁵ Departament de Química, Universitat Autònoma de Barcelona, Cerdanyola del Vallès, 08193

Barcelona, Spain.

Keywords: Hydrogen, electrocatalytic nanomaterial, molecular catalyst, solar fuels, carbon nanotubes.

The anticipated shortage of an increasing number of critical elements, especially metals, requires a shift towards molecularly-defined materials with low metal loadings. More particularly, surface-anchored molecular catalysts are attractive to prospectively enable cost-effective electrochemical hydrogen evolution. However, the design of ligands integrating specific anchoring unit(s) for the immobilization of molecular catalysts can be challenging and has direct consequences on the intrinsic properties of the grafted complex. In this work, two cobalt tetraazamacrocyclic complexes, bearing pyrene anchoring groups at different positions on the macrocyclic ligands were synthesized. The pyrene unit allows for simple immobilization and electrochemical characterization of the two complexes on multiwalled carbon nanotube-based electrodes. Thorough electrochemical and electrocatalytic investigation demonstrates important differences between the two closely-related catalysts in terms of catalyst loading, catalytic response and stability over time, with a significantly higher stability observed at pH 7 than at pH 2.



Introduction

The necessary global energy transition towards reliance on sustainable energy sources is driving a push for the production of clean fuels able to conveniently and efficiently store the harvested renewable – but intermittent – energy. Currently, Hydrogen (H_2) represents one of the most promising potential solar fuels, due to its high energy density per mass, relative simplicity to produce from an abundant resource, and re-conversion to electricity when combined with oxygen in fuel cells to only produce water as a by-product.¹ Sustainable and scalable production of H_2 from electrolyzers will require further development of efficient and stable catalysts based on widely available materials,^{2,3} and their effective incorporation into integrated systems.^{4,5} Currently however, most electrolyzer technologies still heavily rely on the use of scarce platinum-group metals (PGMs) as H_2 production and H_2O oxidation catalysts.^{6–8} In that context, the development of bio-inspired hydrogen-evolving molecular catalysts represents an appealing approach to enable the replacement of PGMs with earth-abundant first-row transition metals, while limiting the overall metal content, to improve the metal atom economy.^{9–12} This field of research has been very active over the past two decades, and the development of such catalysts has been extensively reported in the literature.^{13,14} The vast modularity of molecular engineering is exploited to increase

the catalytic performances and stability of the metal-centered active site, by tuning the critical steric and electronic effects from the inner and outer coordination spheres.¹⁵⁻¹⁷ Recent achievements made with cobalt-polypyridyl and cobalt-aminopyridyl complexes have resulted in robust and efficient catalysts under aqueous electrocatalytic and photocatalytic conditions.¹⁸⁻²⁰ Indeed, such ligand frameworks efficiently accommodate the different redox states of the catalytic cycle, thus preventing demetallation that can occur in the lowest oxidation states; they are also less prone to hydrolysis under acidic conditions, a drawback frequently encountered with the cobaloxime and cobalt diimine-dioxime catalysts.²¹⁻²³ Finally, the presence of redox-active moieties and proton relays within the vicinity of the cobalt center can help in promoting, tuning and/or improving the catalytic activity according to the operating conditions.²⁴⁻²⁶ All these features therefore make these catalysts excellent candidates for further integration into water-splitting devices, typically through heterogenization at electrode surfaces, to develop useful, stable and scalable electrocatalytic cathode materials.^{13,27,28}

A representative example of this family of catalysts is the cobalt tetraazamacrocyclic complex $[\text{Co}(\text{N}_4\text{H})\text{Cl}_2]^+$ (**1**, $\text{N}_4\text{H} = 2,12\text{-dimethyl-}3,7,11,17\text{-tetraazabicyclo}[11.3.1]\text{heptadeca-}1(17),2,11,13,15\text{-pentaene}$), which has been shown to be an effective catalyst for the hydrogen evolution reaction (HER) in organic solvents as well as under fully aqueous conditions.²⁹⁻³⁴ Recently, **1** has received a lot of interest because of its potential for structural modification to optimize its catalytic properties for the HER^{35,36} and the related carbon dioxide reduction reaction (CO₂RR),³⁷ and also in the context of photoelectrochemical hydrogen production.^{38,39} So far, however, anchoring of **1** onto electrodes for direct electrocatalytic production of H₂ from water has not yet been reported.

Electrode immobilization in most cases implies structural modification at the ligand and/or metal coordination sphere which can impact the intrinsic redox and electrocatalytic properties of the final catalyst compared to its parent counterpart. In addition, the selection of an appropriate electrode material is important for integration of the H₂-evolving catalysts into devices. Multiwalled carbon nanotubes (MWCNTs) represent a very convenient choice of electrode material for molecular electrocatalysis applications, due to their very large specific surface areas and excellent conductivity, which allow high surface loadings of active centers to be reached without the loss of electron transfer efficiency between the pi-conjugated surface and the catalyst.^{40,41} Moreover, their surface can be chemically modified by numerous covalent or non-covalent strategies, making them versatile nanoplatforms for molecular catalyst integration.⁴² In particular, in recent years, non-covalent modifications of MWCNTs with pyrene-bearing molecular catalysts have been widely employed as a smooth and efficient approach to carry out numerous electrocatalytic processes, such as H₂ evolution^{10,43–45} and oxidation,^{12,46} CO₂ reduction^{47–49} and even water oxidation.^{50–52}

In this work we describe the development of two original derivatives of the catalyst **1**, each functionalized with a pyrene anchoring group either through a rigid benzamidomethyl bridge in *para*-position of the pyridine moiety (**2** in Figure 1) or through a methylene bridge linked to the coordinated amine on the opposite side of the macrocyclic ligand (**3** in Figure 1). Full electrochemical characterization of MWCNT-based electrodes functionalized with **2** and **3** were performed together with controlled potential electrolysis experiments in order to shed light on the distinct performances obtained depending on the position of substitution on the catalytic unit.

Results and Discussion

Synthesis and characterization of complexes 2 and 3. Complex **2** was synthesized via 5 consecutive steps, starting from commercially available chelidamic acid. Briefly, introduction of a protected benzoic acid group in the *para* position of the diiminopyridine-based ligand was achieved through a palladium-catalyzed cross-coupling reaction prior to the templated synthesis of the macrocyclic catalytic core, removal of the protecting group, and an amide coupling with 1-pyrenemethylamine to yield the pyrene-appended catalyst **2** in Co^{III} oxidation state, analogous to **1**. The synthetic route towards **3** starts with the nucleophilic substitution of 1-bromomethylpyrene by a protected derivative of bis-(3-aminopropyl)amine. A deprotection step, followed by a template synthesis with Co(NO₃)₂ in MeOH yields the air-stable Co^{II} macrocyclic complex. Full synthetic details and characterizations are provided in the Supporting Information (Figures S1, S2). Prior to electrode integration, the electrochemical properties of the new complexes **2** and **3** were determined by cyclic voltammetry (CV) in dry and degassed *N,N*-dimethylformamide (DMF) and compared to those of the parent complex **1** in order to evaluate the possible effects from the introduction of the pyrene anchor (Figure 1).

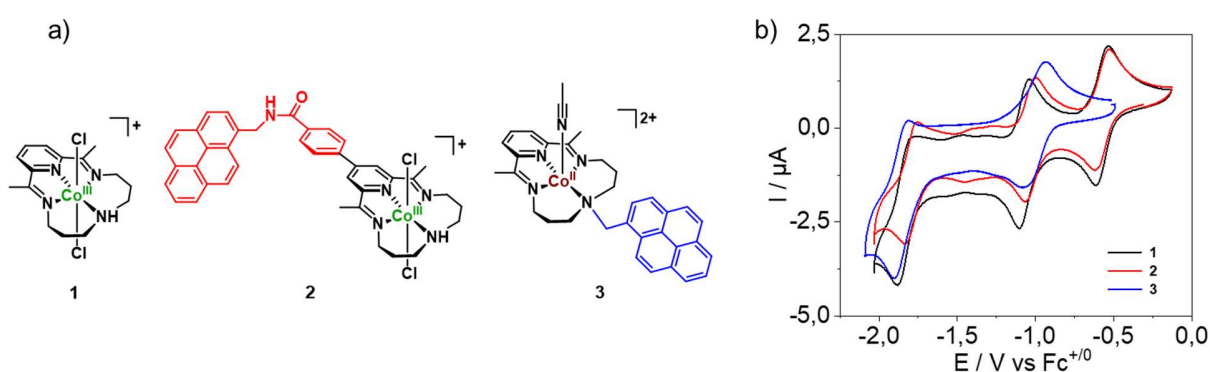


Figure 1. a) Chemical structures of complexes **1**, **2** and **3** in their air-stable oxidation states; b) CVs of complexes **1**, **2** and **3** recorded at 100 mV s⁻¹ at a glassy carbon electrode (Supporting electrolyte: 0.1 M TBABF₄ in dry DMF).

The CV of the Co^{III} complex **2** displays redox features very similar to the ones recorded for **1** under the same conditions, with three successive events on the cathodic scan assigned to the Co^{III/II} ($E_{1/2} = -0.57$ V vs Fc⁺⁰ for **1** and **2**), the Co^{II/I} ($E_{1/2} = -1.07$ and -1.03 V vs Fc⁺⁰ for **1** and **2**, respectively) and the ligand-centered L/L⁻ ($E_{pc} = -1.83$ and -1.79 V vs Fc⁺⁰ for **1** and **2**, respectively) redox couples.^{31,35} The slight anodic shift observed for the Co^{II/I} and the ligand-based processes can be explained by the introduction of the benzamido substituent at the *para* position of the pyridine ring having an electron-withdrawing character and extending the conjugation of the ligand, as observed recently for parent Co complexes.³⁷ On the other hand, the Co^{II} complex **3** shows only one Co centered redox process at $E_{1/2} = -0.98$ V vs Fc⁺⁰, assigned to the Co^{II/I} redox couple, while the redox system at $E_{1/2} = -1.86$ V vs Fc⁺⁰ is attributed to the ligand-centered process; these potentials are very close to the ones previously reported for the related *N*-methyl-functionalized catalyst.³⁵

Preparation and electrochemical characterization of 2|MWCNT and 3|MWCNT. To investigate the electrocatalytic activity of complexes **2** and **3** for hydrogen production in aqueous medium, modified electrodes were prepared by drop-casting a suspension of MWCNTs in ethanol onto glassy carbon disc electrodes, followed by incubation in a DMF solution of the pyrene-appended catalysts (Figure S3).

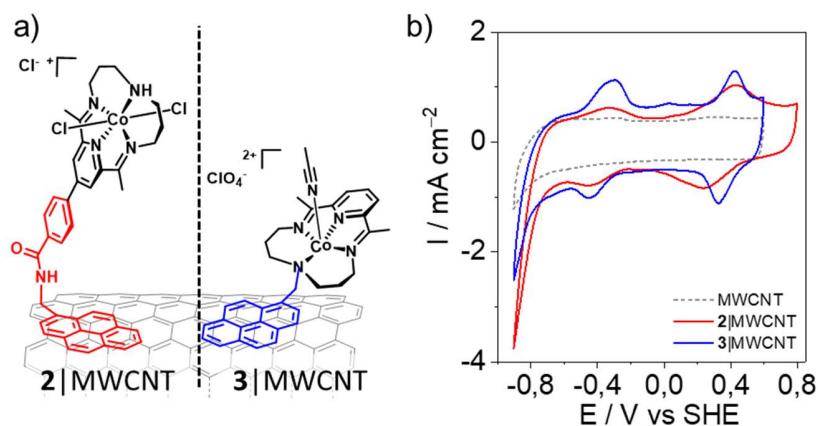


Figure 2. a) Schematic representation of complexes **2** and **3** immobilized onto MWCNTs; b) CVs of bare MWCNT (gray trace), **2**|MWCNT (red trace), and **3**|MWCNT (blue trace) modified electrodes recorded in KPi 0.1M pH 7, under nitrogen (100 mV s^{-1}).

CVs experiments were first conducted in pH 7 aqueous 0.1 M potassium phosphate buffer (KPi) electrolyte, in order to compare the redox properties of **2**|MWCNT and **3**|MWCNT. Both electrodes exhibit a well-defined $\text{Co}^{\text{III/II}}$ redox couple at $E_{1/2} = +0.33 \text{ V vs SHE}$ ($\Delta E = 197 \text{ mV}$) and $E_{1/2} = +0.38 \text{ V vs SHE}$ ($\Delta E = 98 \text{ mV}$) for **2**|MWCNT and **3**|MWCNT, respectively, with the peak current varying linearly with the scan rate up to 0.2 V s^{-1} , as expected for a surface-confined redox process (Figures S4–S5). This process is quasi-reversible for **3**, in agreement with a fast displacement of the axial acetonitrile ligand by a water molecule; by contrast, it becomes slower for **2** in aqueous medium (Figure 2b) compared to in organic one (Figure 1b), which is most likely associated with a slow exchange process of the chlorido ligand in the Co coordination sphere.⁵³ Analysis of the electron transfer rate was performed using the Laviron method,⁵⁴ relying on the study of the evolution of peak potential differences with the scan rate. From the corresponding trumpet plots, k_{app} of 0.9 and 4.3 s^{-1} could be obtained for **2**|MWCNT and **3**|MWCNT, respectively (Figure S6, see SI for details). These results lie in the same range as previously measured k_{app} for

adsorbed species at porous electrodes.⁵⁵ The difference in the interfacial electron transfer rate for the two complexes can be rationalized by the difference in the length and nature of the linker separating the cobalt center from the MWCNT electrode surface.

When scanning at more negative potential, the $\text{Co}^{\text{III/I}}$ couple is clearly observed at $E_{1/2} = -0.39$ V vs SHE and -0.37 V vs SHE for **2**|MWCNT and **3**|MWCNT, respectively; this indicates that, for both complexes under these experimental conditions (100 mV s^{-1} at pH 7), the Co^{I} state is not reactive for protonation to generate a Co^{III} hydride and initiate hydrogen production. And indeed, a catalytic wave develops at more negative potentials below -0.6 V vs SHE, most likely close to the ligand-centered process which is not observed anymore under these aqueous conditions. Of note, this wave is observed at a slightly less negative potential for **2**|MWCNT compared to **3**|MWCNT, in agreement with the slight anodic shift observed for the ligand-based process in **2**, due to the electron-withdrawing character of the benzamido substituent introduced at the *para* position of the pyridine ring.

In order to further investigate the electrochemical behavior and reactivity of both systems in aqueous media, CVs were recorded at different pH values ranging from 2 to 9 using the Britton-Robinson universal buffer (Figure 3a–b, S7 and S8). From these data, Pourbaix diagrams positioning the Co species in their different protonation states were plotted for each functionalized electrode (Figure 3c and d). For **3**|MWCNT, a $68 \text{ mV per pH unit}$ dependence is observed for the $\text{Co}^{\text{III/Co}^{\text{II}}}$ redox process at pH higher than ≈ 3 , which is characteristic for a $1\text{e}^-/1\text{H}^+$ process and consistent with a protonation occurring on one of the ligands (L) surrounding the cobalt(III) center upon reduction. This behavior is in perfect agreement with the pH dependence previously reported for **1** in aqueous medium.³⁰ On the other hand, at $\text{pH} < 3$, the Co^{III} species is protonated and the $\text{LH-Co}^{\text{III/LH-Co}^{\text{II}}}$ potential remains constant at 0.70 V vs SHE. For **2**|MWCNT, thermodynamic

stability is observed for the protonated LH-Co^{III} species on a wider range of pH, up to pH \approx 4.5. At higher pH values, a 46 mV per pH unit dependence for the Co^{III/II} redox process is measured; although not canonical and probably stemming from a slow Cl⁻/OH₂ axial ligand exchange on **2**, this behavior also indicates a proton-coupled electron transfer (PCET). For both complexes, the Co^{III}/Co^{II} process remains fairly reversible, pointing to a fast and equilibrated protonation reaction. Although no straightforward conclusion can be drawn from the data presented here, this protonation occurs either on the hydroxo ligand (Co^{III}-OH/Co^{II}-OH₂ equilibrium) or at the coordinated amine group, the latter having been previously proposed in several studies.^{30,31,35}

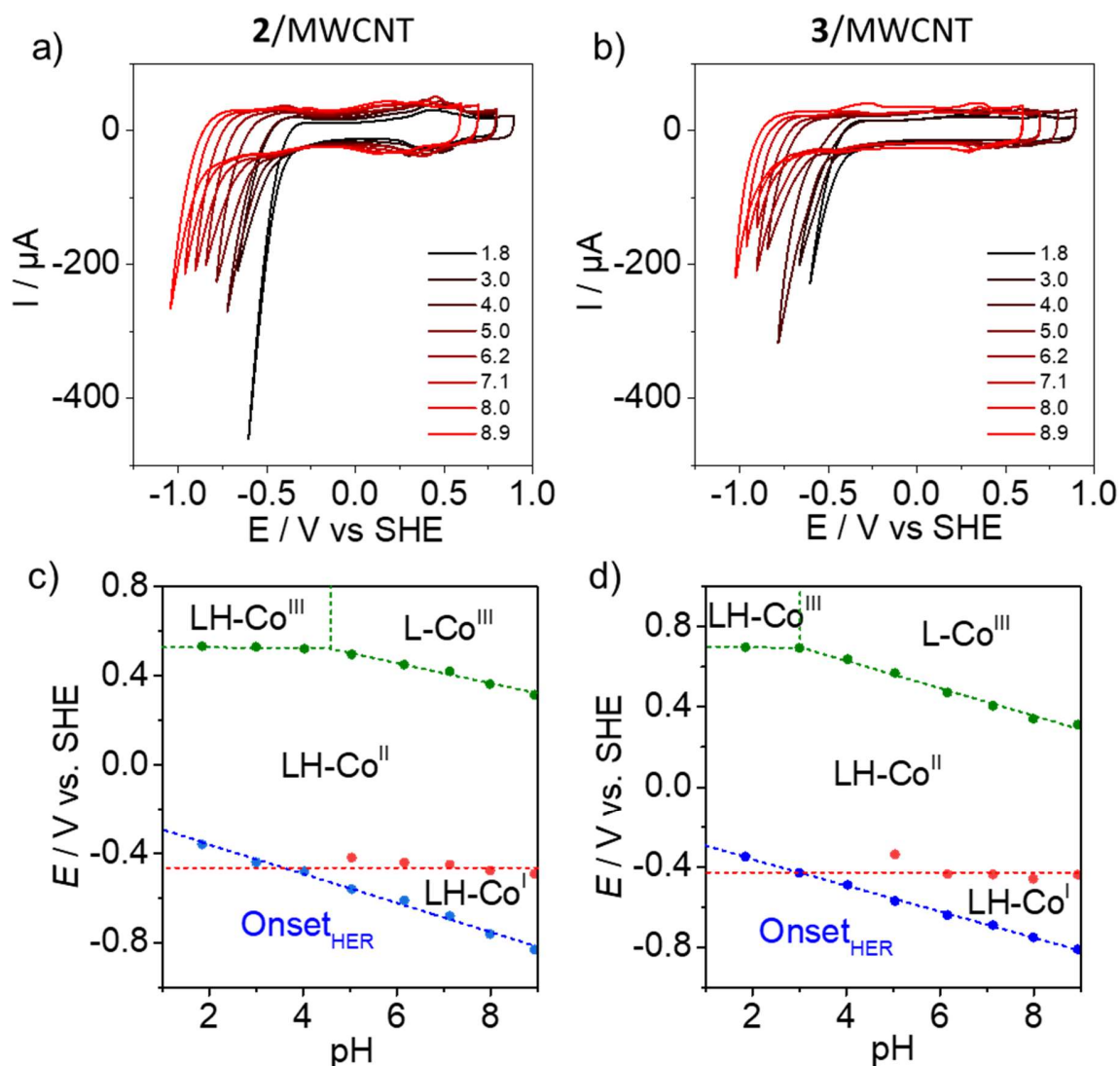


Figure 3. a) and b) CVs of **2**/MWCNT and **3**/MWCNT over different potential ranges and at pH values ranging from 2 to 9 in Britton-Robinson buffer ($v = 20 \text{ mV s}^{-1}$). c) and d) Pourbaix diagrams of **2** and **3**, anchored onto MWCNTs electrodes

Looking at more negative potential values, two different situations arise depending on the pH. At neutral to basic pH, the LH-Co^{II}/LH-Co^I couple is observed without any significant pH dependence (Figures 3, S7b, S8b). As described above for the measurements at pH 7 in KPi buffer, the catalytic wave develops beyond the Co^{II}/Co^I redox couple, indicating that an additional

reduction step forming the $\text{LH}^{\bullet}\text{-Co}^{\text{I}}$ intermediate is necessary to initiate catalysis. A 60 mV per pH unit dependence is observed for the catalytic wave, consistent with the occurrence of a $1\text{e}^{-}/1\text{H}^{+}$ coupled process at that stage. By contrast, at more acidic pH values, the $\text{LH-Co}^{\text{II}}/\text{LH-Co}^{\text{I}}$ redox couple is no longer detected and the catalytic wave develops instead. This is highlighted on Figure S9, with CVs plotted at selected pH values, either acidic (pHs 2 and 3), or neutral to slightly basic (pHs 6, 7 and 8), to underline this difference in behavior, similarly occurring for both complexes.

Taken altogether, these observations lead to two plausible mechanisms for hydrogen production catalyzed by **2**|MWCNT and **3**|MWCNT depending on the pH of the medium (Figure 4). From basic to slightly acidic conditions, hydrogen production follows an EECC reaction scheme (where E stands for an electrochemical step, *i.e.* reduction, and C for a chemical one, *i.e.* protonation or hydrogen evolution): Reduction of LH-Co^{II} yields first LH-Co^{I} . This is followed at more negative potentials by a second reduction process coupled to protonation to form the hydride $\text{LH-Co}^{\text{II}}\text{-H}$; the latter reacts with a further proton and hydrogen is evolved, regenerating LH-Co^{II} (Figure 4a). When the pH decreases, the two waves come close and finally merge around pH 3. At this point a second mechanism becomes likely where hydrogen production follows an alternative ECEC reaction scheme: reduction of the protonated Co^{II} intermediate (LH-Co^{II}) yields LH-Co^{I} , which is protonated to form the hydride $\text{LH-Co}^{\text{III}}\text{-H}$. As for other H_2 -evolving molecular complexes,⁵⁶⁻⁵⁹ the latter is then reduced to generate the Co^{II} hydride $\text{LH-Co}^{\text{II}}\text{-H}$,^{32,35} which is responsible for the release of H_2 and regeneration of LH-Co^{II} (Figure 4b). A similar mechanism was previously proposed for hydrogen production from **1** in organic medium in the presence of *p*-cyanoanilinium tetrafluoroborate.³¹ Of note, on the sole basis of electrochemical data, it is not possible to distinguish between EECC and ECEC mechanisms.⁶⁰ The rate-determining step of this molecular system, studied under homogeneous conditions in organic medium, has previously been proposed

to be the protonation or intramolecular rearrangement of the $\text{LH-Co}^{\text{II}}\text{-H}$ intermediate to form H_2 .

³¹ Whether the proton located on the ligand actually plays a role in the hydrogen evolution mechanism via an intramolecular protonation step (dashed arrows in Figure 4), as proposed in acidic non-aqueous conditions,³¹ or just acts as a spectator can, however, also not be deciphered from the data collected here.

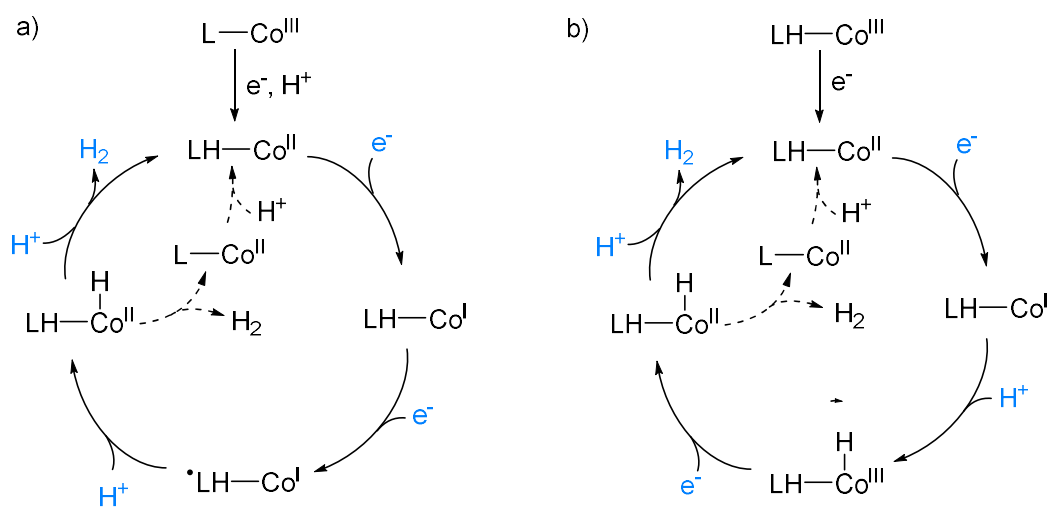


Figure 4: Mechanisms proposed for the electrocatalytic production of H_2 with **2**|MWCNT and **3**|MWCNT under a) neutral conditions and b) acidic conditions (the overall charge of the complex is omitted for clarity).

The two complexes anchored onto MWCNTs thus display very similar catalytic behavior, suggesting that the two different structural modifications used to introduce the pyrene anchoring group do not significantly impact their catalytic ability, apart from a slightly less negative onset potential for catalysis at pH 7 with **2**|MWCNT.

Determination of catalyst surface loading. Integration of the oxidation wave of the $\text{Co}^{\text{III/II}}$ redox couple of the CVs allowed the quantification of the electrochemically active Co centers.

Respectively 17.0 ± 1.0 and 9.4 ± 2.0 nmol.cm⁻² of adsorbed **2** and **3** were quantified electrochemically. The significantly lower catalyst loading obtained with **3** is tentatively attributed to the shorter linker between the pyrene group and the cobalt tetraazamacrocyclic unit, placing the Co center closer to the surface and resulting in steric constraints (Figure 2a), and/or to the different solubility of the complexes, resulting in different equilibria during the anchoring process. For comparison, Co loadings were also quantified by ICP-AES (see SI for details) for the MWCNT electrodes modified with **2** (**2**|MWCNT) and **3** (**3**|MWCNT) and surface concentrations of 28.9 ± 3.2 nmol.cm⁻² and 15.3 ± 1.9 nmol.cm⁻² were obtained, respectively. While the differences in loading between **2** and **3** remain similar, a significant discrepancy is observed between the electrochemical and ICP values. These results suggest that a non-negligible part of the cobalt (around 40% for both complexes) is apparently not electrochemically detectable; although the reasons for this behavior are still unclear, a strong electronic coupling between the complex and the electrode material, as reported recently for a Co-porphyrin HER catalyst, could be invoked.^{62,63} Such an interaction is plausible, as illustrated in the crystal structure of **3**, presenting a short Co-C_{pyrene} distance of 2.80 Å (see Figures S2 in the SI).

Electrocatalytic hydrogen production activity assessment. Controlled potential electrolysis (CPE) experiments were performed to determine the Faradaic Efficiency (FE) for H₂ production and to assess the stability of **2**|MWCNT and **3**|MWCNT under both acidic (pH 2, 0.1M KCl/HCl electrolyte) and neutral (pH 7, 0.1M KPi electrolyte) conditions (Figure 5).

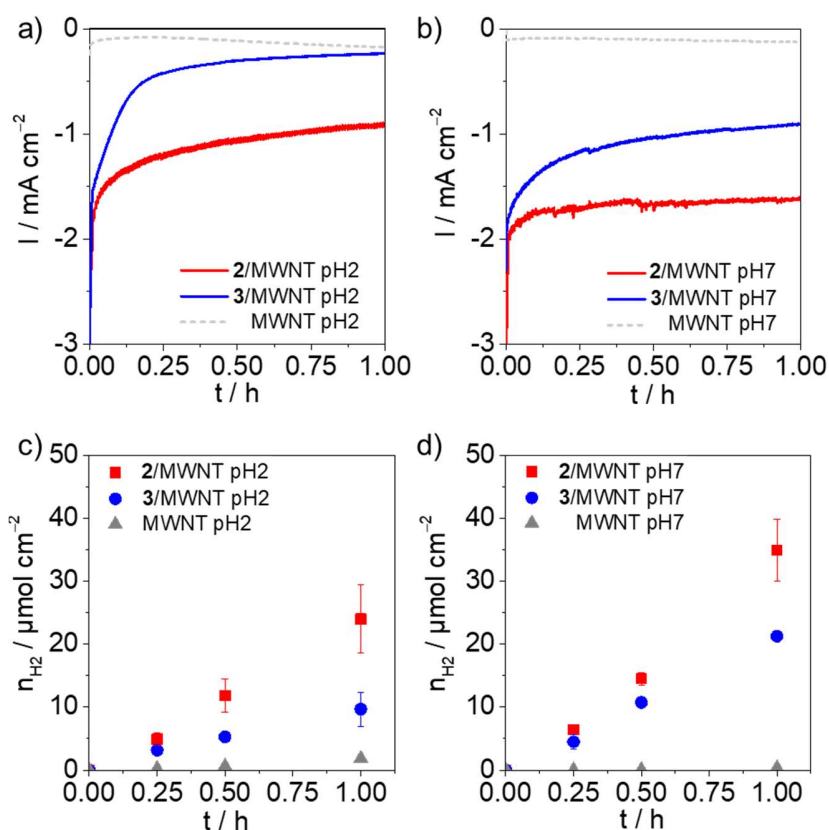


Figure 5. Top: CPE measurements recorded on 2|MWCNT (red traces), 3|MWCNT (blue traces) and bare MWCNT (grey dotted traces) at an applied potential of a) -0.6 V vs SHE in KCl/HCl 0.1 M at pH 2 and b) -0.9 V vs SHE in 0.1 M KPi at pH 7. Bottom: Amount of H_2 produced as a function of time at 2|MWCNT (red squares), 3|MWCNT (blue dots) and bare MWCNT (grey triangles) at c) -0.6 V vs SHE in KCl/HCl 0.1M at pH 2 and d) -0.9 V vs SHE in 0.1 M KPi at pH 7. All measurements were performed under N_2 .

At pH 2, different current responses can be observed for 2|MWCNT and 3|MWCNT (Figure 5a, Figure S10). While both electrodes generate similar initial current densities of around -2 mA cm^{-2} (Table S2) after initial stabilization, the current sharply decreases during the first 10 minutes of the experiment for 3|MWCNT, and reaches the background values recorded on a bare MWCNT electrode at the end of the CPE experiment. By contrast, the current produced at 2|MWCNT decays

much slowly, 50% being maintained after one hour. Sampling the headspace of the working electrode compartment, H₂ was quantified by gas chromatography. Under these conditions (pH 2, Figure 5c), H₂ is steadily produced during the course of the experiment, up to $23.7 \pm 5.4 \mu\text{mol}_{\text{H}_2} \text{cm}^{-2}$ after 1 h CPE, corresponding to a Faradaic efficiency (FE_{H₂}) of $98 \pm 2 \%$ and a TON_{H₂} of 821 ± 186 for **2**|MWCNT (Figure S12, Table S2). On the other hand, the production of H₂ with **3**|MWCNT quickly levelled off to reach $9.6 \pm 2.7 \mu\text{mol cm}^{-2}$ after 1 h with a slightly lower FE_{H₂} of $93 \pm 7 \%$, hinting at a faster loss of activity for the **3**|MWCNT electrode.

Performing the same series of experiments in neutral pH conditions (pH 7) allowed to observe a much more sustained activity for **2**|MWCNT (Figure 5b, Figure S11). After 1 h CPE, a steady current density of $-1.7 \pm 0.2 \text{ mA cm}^{-2}$ at E_{app} = -0.9 V vs SHE is recorded, corresponding to more than 80% of the initial value. Here, less stable current responses were again obtained with **3**|MWCNT, decreasing from -1.7 to $-1.0 \pm 0.1 \text{ mA cm}^{-2}$ within 1 h, thus retaining only about 60% of catalytic activity. Importantly, the production of H₂ remained stable during the course of the electrolysis for both **2**|MWCNT and **3**|MWCNT, reaching $34.5 \pm 4.9 \mu\text{mol cm}^{-2}$ and $21.0 \pm 0.7 \mu\text{mol cm}^{-2}$ of H₂, respectively, with FE_{H₂} of 100 % (Table S2). Based on the catalyst loadings determined above, TON_{H₂} calculated for **2**|MWCNT and **3**|MWCNT reach 1195 ± 169 and 1375 ± 44 , respectively, after 1 h CPE. The higher TONs obtained with **3**|MWCNT need to be put in perspective with the much lower surface loading. Importantly, control CPE experiments performed on bare MWCNT electrodes only generated small amounts of H₂, 1.8 and $0.3 \mu\text{mol cm}^{-2}$ at pH 2 and 7, respectively, confirming that the H₂ evolution activity stems from the presence of the molecular Co complexes (Figure 5).

CV measurements were performed post-electrolysis in order to gain insight into the molecular integrity of the molecular catalyst at the electrode surface. At pH 2, the CV response of **2**|MWCNT

shows a drastic decrease in surface loading of **2**, with only 14.3 ± 5.7 nmol cm⁻² of electrochemically active complex remaining after 1 h, *i.e.* less than 60% of the initial surface concentration (Figure S13a, 54% from ICP-AES quantification). In parallel, the Co^{III}/Co^{II} redox response also shifted towards more negative potential, implying a change in the coordination environment of the Co center. The Co^{II}/Co^I couple was not visible in the same potential window and the catalytic wave was notably smaller, in coherence with the CPE results where the electrocatalytic response dropped by about 60%. Post-operando, the **3**|MWCNT modified electrode did not display noticeable redox activity anymore in CV measurement, except for a sharp irreversible process at $E_{ox} = 0.35$ V vs SHE (Figure S13b), believed to be stemming from a polluting source in the electrolyte, as the same process was observed on the control CPE experiment performed on a bare MWCNT electrode (Figure S13c). This complete loss of activity is supported by cobalt quantification by ICP-AES, which shows that only 12% (1.8 ± 0.5 nmol cm⁻²) of the initial amount of cobalt present at the surface of the electrode remains at the end of the 1 h CPE experiment, highlighting sharp differences in the operando stability for the two systems (Table S2).

On the other hand, the CV performed post-CPE at neutral pH on **2**|MWCNT shows a retention of nearly 80% of the initial surface concentration in electroactive species (69% of the initial Co loading from ICP-AES analysis, see Table S2), in line with the CPE results (Figure S14a). Again, a slight negative potential shift of the Co^{III}/Co^{II} redox couple ($E_{1/2} = 0.34$ V vs SHE) was observed along with the disappearance of the Co^{II}/Co^I process, as observed at pH 2 and tentatively attributed to a change in the coordination environment of the Co complex, which was still catalytically active according to the sustained H₂ production activity observed under these conditions. Here again, a more significant amount of Co is lost for **3**|MWCNT with only 28% of the initial Co loading

remaining after the experiment per ICP-AES analysis (Table S2). Of note, the CV recorded post-operando shows negligible redox signature of **3** (Figure S14b), while the electrocatalytic response of **3**|MWCNT for H₂ evolution at pH 7 still shows activity after 1 h of CPE (close to 1 mA cm⁻², Figure 5b and d).

Discussion. Overall, on the basis of the data obtained from CV and CPE measurements, it appears that **2**|MWCNT and **3**|MWCNT catalyze HER over a wide range of pH values with overpotential values of 400 mV and 410–450 mV measured at 2 mA cm⁻² for **2**|MWCNT and **3**|MWCNT, respectively. The slightly lower overpotential requirement observed for **2** is directly linked to the presence and the electron-withdrawing nature of the amido group at the phenyl ring attached to the pyridine ligand that shifts the catalytic response of **2** by 10 mV at pH 7 as compared to **3** (Figure 2).

Taking a closer look at the intrinsic performances delivered by **2** and **3**, both complexes generate very similar initial current densities ($j_{1\text{min}}$ in Table S2) despite the fact that the catalyst surface loading (determined by ICP-AES) is almost twice as much for **2**. This observation suggests that **3** can produce H₂ faster than **2**, and, indeed, we estimate TOF values on the basis of the current density $j_{1\text{min}}$ recorded at 1 min of electrolysis (assuming 100% FE as determined above), which indicates a slightly higher intrinsic activity toward HER for **3** compared to **2**: 0.64 vs 0.36 s⁻¹ at pH 2 and 0.57 vs 0.38 s⁻¹ at pH 7, for **3**|MWCNT and **2**|MWCNT, respectively. We note that for both catalysts slower TOFs are observed compared to the interfacial electron transfer rates measured above, confirming that electron transfer does not limit catalysis. This trend follows the classical linear free-energy relationship between TOF and overpotential requirement observed in most series of molecular catalysts with a decrease in overpotential requirement occurring at the

expense of the TOF value.⁶⁴ Interestingly, the lower intrinsic turnover frequency of **2**|MWCNT compared to **3**|MWCNT is counterbalanced by the higher loading allowed by a more flexible linker: the longer linker in **2** places the Co center away from the surface, which favors a more compact radial assembly around the nanotube surfaces. By contrast, appending the pyrene anchor on the amine group in **3** induces stronger steric constraints on the cobalt coordination sphere and may result in a larger footprint of **3** vs **2**.

For both materials, however, working under acidic conditions comes at the expense of electrode stability. Indeed, more stable current densities are recorded at pH 7 for both complexes and a higher amount of remaining Co is quantified at the end of the CPE experiment. We established that two different catalytic mechanisms can be at play, depending on the pH value: an ECEC mechanism based on the formation of the Co(III)-H intermediate at pH 2 vs an EECC pathway involving reduction of the ligand at pH 7. As Co(III)-H species are known to be potent hydride donors to unsaturated Co ligands,^{65,66} their involvement as intermediates in the ECEC mechanism could be a plausible explanation for the faster deactivation observed at pH 2. In addition, the amount of Co lost from the electrode surface during the course of the CPE experiments is clearly higher for **3** (\approx 90% at pH 2 and 70% at pH 7) than for **2** (\approx 50% at pH 2 and 30% at pH 7), highlighting striking differences in terms of stability for **2**|MWCNT and **3**|MWCNT. Here also, this could be due to structural constraints limiting the ability of **3**|MWCNT to accommodate the different intermediates of the catalytic cycle (amine protonation included), which could in turn induce faster degradation.

Interestingly, a non-negligible fraction of Co loaded on the electrode is not detected in the CV for each system both before and after catalysis. This is especially observed for catalyst **3** at pH 7, where the redox signature of the complex is hardly detected post-operando (Figure S14b), while

the electrode is still active for H₂ production, with a current density of 1 mA cm⁻² reproducibly recorded after one hour (Figure S11b). This remaining activity could stem from the presence of active Co centers electronically coupled to the electrode material that do not exhibit clear redox signatures in the CV measurements, as previously observed for a Co porphyrin covalently grafted to a glassy carbon electrode.⁶² This phenomenon is more likely to occur for **3** than for **2**, due to the restricted geometry and shorter linkage between the pyrene group and the cobalt catalytic center of the former (Figure S2).

Conclusions

In this work, we have described the synthesis and full characterization of two novel derivatives, **2** and **3**, of the hydrogen-evolving complex [Co(N₄H)Cl₂]⁺ (**1**), functionalized with a pyrene moiety at two different positions on the macrocycle. Following their integration onto MWCNTs-based electrodes through non-covalent π -stacking interactions, the electrocatalytic properties of the two molecular cathodes towards the production of H₂ were tested in both acidic and neutral aqueous conditions. The results are informative on how the electronic nature of the linker holding the pyrene group, its position and its flexibility can impact the redox and catalytic responses, as well as the stability and overall HER performance of the prepared hybrid electrodes. In particular, the presence of the amido group at the phenyl group directly connected to the pyridine leads to a slightly lower overpotential requirement for HER and a lower TOF value. This lower intrinsic TOF is compensated with a higher loading of active sites, owing to the longer and bulkier linker in **2** compared to the short linker attached to the coordinating amine in **3** and the more constrained geometry this entails. Overall, the **2**|MWCNT electrode performs slightly better than **3**|MWCNT and also displays greater stability under cycling, especially under neutral conditions, warranting a

deeper investigation of such conditions, including electrolyte engineering,^{67,68} for water electrolysis.

Overall, this study highlights the importance of selecting suitable linkers and integrating them at appropriate positions on the ligand frameworks of molecular catalysts. It remains however highly challenging to address all the parameters that are modified upon varying the anchoring group position and the linker nature. Any subtle change in the length, conjugation, flexibility of the linker or in the electronic structure of the metal center will in turn influence interfacial electron transfer processes, as well as the reactivity of the catalytic center. More systematic investigations on the linker's nature would allow to clarify how it can influence heterogeneous molecular catalysis. Finally, deciphering how the local environment and possible electronic coupling with the electrode material can affect the activity and the stability of heterogenized molecular catalysts will also be key for the effective integration of Earth-abundant molecular complexes into sustainable fuel-producing devices.

AUTHOR INFORMATION

Corresponding Author

*Vincent Artero, vincent.artero@cea.fr

Author Contributions

The manuscript was written through contributions of all authors. All authors have given approval to the final version of the manuscript. ‡These authors contributed equally.

ASSOCIATED CONTENT

Supporting Information. The following files are available free of charge. Detailed synthetic procedures, XRD data for complex **3** (CCDC Deposition Number 2314693) and additional electrochemical data (PDF).

Funding Sources

This work received funding from the European Union's Horizon 2020 Research and Innovation program under grant agreement no. 765376 (eSCALED Marie Curie ITN project) and was partly supported by the French National Research Agency (Labex ARCANE, CBH-EUR-GS, ANR-17-EURE-0003), the Ministry of Science and Innovation of Spain MICINN (PID2022-140143OB-I00 to AL, PID2021-128496OB-I00 and RYC2019-027423-I to CGS), Generalitat de Catalunya-AGAUR (2017SGR1631 and 2021SGR00064) and Severo Ochoa (CEX2019-000925-S).

REFERENCES

- (1) Faunce, T.; Styring, S.; Wasielewski, M. R.; Brudvig, G. W.; Rutherford, A. W.; Messinger, J.; Lee, A. F.; Hill, C. L.; deGroot, H.; Fontecave, M.; MacFarlane, D. R.; Hankamer, B.; Nocera, D. G.; Tiede, D. M.; Dau, H.; Hillier, W.; Wang, L.; Amal, R. Artificial Photosynthesis as a Frontier Technology for Energy Sustainability. *Energy Environ. Sci.* **2013**, *6* (4), 1074. <https://doi.org/10.1039/c3ee40534f>.
- (2) Oliveira, A. M.; Beswick, R. R.; Yan, Y. A Green Hydrogen Economy for a Renewable Energy Society. *Curr. Opin. Chem. Eng.* **2021**, *33*, 100701. <https://doi.org/10.1016/j.coche.2021.100701>.
- (3) Velazquez Abad, A.; Dodds, P. E. Green Hydrogen Characterisation Initiatives: Definitions, Standards, Guarantees of Origin, and Challenges. *Energy Policy* **2020**, *138*, 111300. <https://doi.org/10.1016/j.enpol.2020.111300>.
- (4) Ringsmuth, A. K.; Landsberg, M. J.; Hankamer, B. Can Photosynthesis Enable a Global Transition from Fossil Fuels to Solar Fuels, to Mitigate Climate Change and Fuel-Supply Limitations? *Renew. Sust. Energ. Rev.* **2016**, *62*, 134–163. <https://doi.org/10.1016/j.rser.2016.04.016>.
- (5) Montoya, J. H.; Seitz, L. C.; Chakthranont, P.; Vojvodic, A.; Jaramillo, T. F.; Nørskov, J. K. Materials for Solar Fuels and Chemicals. *Nat. Mater.* **2017**, *16* (1), 70–81. <https://doi.org/10.1038/nmat4778>.
- (6) Vesborg, P. C. K.; Jaramillo, T. F. Addressing the Terawatt Challenge: Scalability in the Supply of Chemical Elements for Renewable Energy. *RSC Adv.* **2012**, *2* (21), 7933–7947. <https://doi.org/10.1039/c2ra20839c>.

- (7) Ardo, S.; Fernandez Rivas, D.; Modestino, M. A.; Schulze Greiving, V.; Abdi, F. F.; Alarcon Llado, E.; Artero, V.; Ayers, K.; Battaglia, C.; Becker, J.-P.; Bederak, D.; Berger, A.; Buda, F.; Chinello, E.; Dam, B.; Di Palma, V.; Edvinsson, T.; Fujii, K.; Gardeniers, H.; Geerlings, H.; Hashemi, S. M.; Haussener, S.; Houle, F.; Huskens, J.; James, B. D.; Konrad, K.; Kudo, A.; Kunturu, P. P.; Lohse, D.; Mei, B.; Miller, E. L.; Moore, G. F.; Muller, J.; Orchard, K. L.; Rosser, T. E.; Saadi, F. H.; Schüttauf, J.-W.; Seger, B.; Sheehan, S. W.; Smith, W. A.; Spurgeon, J.; Tang, M. H.; van de Krol, R.; Vesborg, P. C. K.; Westerik, P. Pathways to Electrochemical Solar-Hydrogen Technologies. *Energy Environ. Sci.* **2018**, *11* (10), 2768–2783. <https://doi.org/10.1039/C7EE03639F>.
- (8) Bullock, R. M.; Chen, J. G.; Gagliardi, L.; Chirik, P. J.; Farha, O. K.; Hendon, C. H.; Jones, C. W.; Keith, J. A.; Klosin, J.; Minteer, S. D.; Morris, R. H.; Radosevich, A. T.; Rauchfuss, T. B.; Strotman, N. A.; Vojvodic, A.; Ward, T. R.; Yang, J. Y.; Surendranath, Y. Using Nature’s Blueprint to Expand Catalysis with Earth-Abundant Metals. *Science* **2020**, *369* (6505), eabc3183. <https://doi.org/10.1126/science.abc3183>.
- (9) Sun, D.; Morozan, A.; Koepf, M.; Artero, V. A Covalent Cobalt Diimine-Dioxime – Fullerene Assembly for Photoelectrochemical Hydrogen Production from near-Neutral Aqueous Media. *Chem. Sci.* **2022**, *13* (13), 3857–3863. <https://doi.org/10.1039/D1SC06335A>.
- (10) Zamader, A.; Reuillard, B.; Marcasuzaa, P.; Bousquet, A.; Billon, L.; Espí Gallart, J. J.; Berggren, G.; Artero, V. Electrode Integration of Synthetic Hydrogenase as Bioinspired and Noble Metal-Free Cathodes for Hydrogen Evolution. *ACS Catal.* **2023**, *13* (2), 1246–1256. <https://doi.org/10.1021/acscatal.2c05175>.
- (11) Zamader, A.; Reuillard, B.; Pérard, J.; Billon, L.; Berggren, G.; Artero, V. Synthetic Styrene-Based Bioinspired Model of the [FeFe]-Hydrogenase Active Site for Electrocatalytic Hydrogen Evolution. *Sustain. Energy Fuels* **2023**, *7* (19), 4967–4976. <https://doi.org/10.1039/D3SE00409K>.
- (12) Schild, J.; Reuillard, B.; Morozan, A.; Chenevier, P.; Gravel, E.; Doris, E.; Artero, V. Approaching Industrially Relevant Current Densities for Hydrogen Oxidation with a Bioinspired Molecular Catalytic Material. *J. Am. Chem. Soc.* **2021**, jacs.1c07093. <https://doi.org/10.1021/jacs.1c07093>.
- (13) Dalle, K. E.; Warnan, J.; Leung, J. J.; Reuillard, B.; Karmel, I. S.; Reisner, E. Electro- and Solar-Driven Fuel Synthesis with First Row Transition Metal Complexes. *Chem. Rev.* **2019**, *119* (4), 2752–2875. <https://doi.org/10.1021/acs.chemrev.8b00392>.
- (14) Berardi, S.; Drouet, S.; Francàs, L.; Gimbert-Suriñach, C.; Guttentag, M.; Richmond, C.; Stoll, T.; Llobet, A. Molecular Artificial Photosynthesis. *Chem. Soc. Rev.* **2014**, *43* (22), 7501–7519. <https://doi.org/10.1039/C3CS60405E>.
- (15) Queyriaux, N.; Kaeffer, N.; Morozan, A.; Chavarot-Kerlidou, M.; Artero, V. Molecular Cathode and Photocathode Materials for Hydrogen Evolution in Photoelectrochemical Devices. *J. Photochem. Photobiol. C: Photochem. Rev.* **2015**, *25*, 90–105. <https://doi.org/10.1016/j.jphotochemrev.2015.08.001>.
- (16) Artero, V. Bioinspired Catalytic Materials for Energy-Relevant Conversions. *Nat. Energy* **2017**, *2* (9), 17131. <https://doi.org/10.1038/nenergy.2017.131>.
- (17) Andreiadis, E. S.; Chavarot-Kerlidou, M.; Fontecave, M.; Artero, V. Artificial Photosynthesis: From Molecular Catalysts for Light-Driven Water Splitting to Photoelectrochemical Cells. *Photochem. Photobiol.* **2011**, *87* (5), 946–964. <https://doi.org/10.1111/j.1751-1097.2011.00966.x>.

- (18) Queyriaux, N.; Jane, R. T.; Massin, J.; Artero, V.; Chavarot-Kerlidou, M. Recent Developments in Hydrogen Evolving Molecular Cobalt(II)–Polypyridyl Catalysts. *Coord. Chem. Rev.* **2015**, *304–305*, 3–19. <https://doi.org/10.1016/j.ccr.2015.03.014>.
- (19) Droghetti, F.; Lucarini, F.; Molinari, A.; Ruggi, A.; Natali, M. Recent Findings and Future Directions in Photosynthetic Hydrogen Evolution Using Polypyridine Cobalt Complexes. *Dalton Trans.* **2022**, *51* (28), 10658–10673. <https://doi.org/10.1039/D2DT00476C>.
- (20) Tong, L.; Duan, L.; Zhou, A.; Thummel, R. P. First-Row Transition Metal Polypyridine Complexes That Catalyze Proton to Hydrogen Reduction. *Coord. Chem. Rev.* **2020**, *402*, 213079. <https://doi.org/10.1016/j.ccr.2019.213079>.
- (21) Dolui, D.; Khandelwal, S.; Majumder, P.; Dutta, A. The Odyssey of Cobaloximes for Catalytic H₂ Production and Their Recent Revival with Enzyme-Inspired Design. *Chem. Commun.* **2020**, *56* (59), 8166–8181. <https://doi.org/10.1039/D0CC03103H>.
- (22) Kaeffer, N.; Chavarot-Kerlidou, M.; Artero, V. Hydrogen Evolution Catalyzed by Cobalt Diimine–Dioxime Complexes. *Acc. Chem. Res.* **2015**, *48* (5), 1286–1295. <https://doi.org/10.1021/acs.accounts.5b00058>.
- (23) Giannoudis, E.; Bold, S.; Müller, C.; Schwab, A.; Bruhnke, J.; Queyriaux, N.; Gablin, C.; Leonard, D.; Saint-Pierre, C.; Gasparutto, D.; Aldakov, D.; Kupfer, S.; Artero, V.; Dietzek, B.; Chavarot-Kerlidou, M. Hydrogen Production at a NiO Photocathode Based on a Ruthenium Dye–Cobalt Diimine Dioxime Catalyst Assembly: Insights from Advanced Spectroscopy and Post-Operando Characterization. *ACS Appl. Mater. Interfaces* **2021**, *13* (42), 49802–49815. <https://doi.org/10.1021/acsami.1c12138>.
- (24) Ginovska-Pangovska, B.; Dutta, A.; Reback, M. L.; Linehan, J. C.; Shaw, W. J. Beyond the Active Site: The Impact of the Outer Coordination Sphere on Electrocatalysts for Hydrogen Production and Oxidation. *Acc. Chem. Res.* **2014**, *47* (8), 2621–2630. <https://doi.org/10.1021/ar5001742>.
- (25) DuBois, D. L. Development of Molecular Electrocatalysts for Energy Storage. *Inorg. Chem.* **2014**, *53* (8), 3935–3960. <https://doi.org/10.1021/ic4026969>.
- (26) Thammavongsy, Z.; Mercer, I. P.; Yang, J. Y. Promoting Proton Coupled Electron Transfer in Redox Catalysts through Molecular Design. *Chem. Commun.* **2019**, *55* (70), 10342–10358. <https://doi.org/10.1039/C9CC05139B>.
- (27) Coutard, N.; Kaeffer, N.; Artero, V. Molecular Engineered Nanomaterials for Catalytic Hydrogen Evolution and Oxidation. *Chem. Commun.* **2016**, *52* (95), 13728–13748. <https://doi.org/10.1039/C6CC06311J>.
- (28) Bullock, R. M.; Das, A. K.; Appel, A. M. Surface Immobilization of Molecular Electrocatalysts for Energy Conversion. *Chem. Eur. J.* **2017**, *23* (32), 7626–7641. <https://doi.org/10.1002/chem.201605066>.
- (29) Leung, C.-F.; Chen, Y.-Z.; Yu, H.-Q.; Yiu, S.-M.; Ko, C.-C.; Lau, T.-C. Electro- and Photocatalytic Hydrogen Generation in Acetonitrile and Aqueous Solutions by a Cobalt Macrocyclic Schiff-Base Complex. *Int. J. Hydrog. Energy* **2011**, *36* (18), 11640–11645. <https://doi.org/10.1016/j.ijhydene.2011.06.062>.
- (30) McCrory, C. C. L.; Uyeda, C.; Peters, J. C. Electrocatalytic Hydrogen Evolution in Acidic Water with Molecular Cobalt Tetraazamacrocycles. *J. Am. Chem. Soc.* **2012**, *134* (6), 3164–3170. <https://doi.org/10.1021/ja210661k>.
- (31) Li, C.-B.; Bagnall, A. J.; Sun, D.; Rendon, J.; Koepf, M.; Gambarelli, S.; Mouesca, J.-M.; Chavarot-Kerlidou, M.; Artero, V. Electrocatalytic Reduction of Protons to Dihydrogen by the Cobalt Tetraazamacrocyclic Complex [Co(N₄H)Cl₂]⁺: Mechanism and Benchmarking of

- Performances. *Sustain. Energy Fuels* **2022**, *6* (1), 143–149. <https://doi.org/10.1039/D1SE01267C>.
- (32) Varma, S.; Castillo, C. E.; Stoll, T.; Fortage, J.; Blackman, A. G.; Molton, F.; Deronzier, A.; Collomb, M.-N. Efficient Photocatalytic Hydrogen Production in Water Using a Cobalt(III) Tetraaza-Macrocyclic Catalyst: Electrochemical Generation of the Low-Valent Co(I) Species and Its Reactivity toward Proton Reduction. *Phys. Chem. Chem. Phys.* **2013**, *15* (40), 17544. <https://doi.org/10.1039/c3cp52641k>.
- (33) Gueret, R.; Castillo, C. E.; Rebarz, M.; Thomas, F.; Hargrove, A.-A.; Pécaut, J.; Sliwa, M.; Fortage, J.; Collomb, M.-N. Cobalt(III) Tetraaza-Macrocyclic Complexes as Efficient Catalyst for Photoinduced Hydrogen Production in Water: Theoretical Investigation of the Electronic Structure of the Reduced Species and Mechanistic Insight. *J. Photochem. Photobiol. B, Biol.* **2015**, *152*, 82–94. <https://doi.org/10.1016/j.jphotobiol.2015.04.010>.
- (34) Roy, S.; Bacchi, M.; Berggren, G.; Artero, V. A Systematic Comparative Study of Hydrogen-Evolving Molecular Catalysts in Aqueous Solutions. *ChemSusChem* **2015**, *8* (21), 3632–3638. <https://doi.org/10.1002/cssc.201501002>.
- (35) Grau Abarca, S.; Schilling, M.; Moonshiram, D.; Benet-Buchholz, J.; Luber, S.; Llobet, A.; Gimbert-Suriñach, C. Electrochemically and Photochemically Induced Hydrogen Evolution Catalysis with Cobalt Tetraazamacrocycles Occurs Through Different Pathways. *ChemSusChem* **2020**, *13* (10), 2745–2752. <https://doi.org/10.1002/cssc.202000283>.
- (36) Lee, C. H.; Villágran, D.; Cook, T. R.; Peters, J. C.; Nocera, D. G. Pacman and Hangman Metal Tetraazamacrocycles. *ChemSusChem* **2013**, *6* (8), 1541–1544. <https://doi.org/10.1002/cssc.201300068>.
- (37) Nie, W.; Tarnopol, D. E.; McCrory, C. C. L. Enhancing a Molecular Electrocatalyst's Activity for CO₂ Reduction by Simultaneously Modulating Three Substituent Effects. *J. Am. Chem. Soc.* **2021**, *143* (10), 3764–3778. <https://doi.org/10.1021/jacs.0c09357>.
- (38) Bold, S.; Massin, J.; Giannoudis, E.; Koepf, M.; Artero, V.; Dietzek, B.; Chavarot-Kerlidou, M. Spectroscopic Investigations Provide a Rationale for the Hydrogen-Evolving Activity of Dye-Sensitized Photocathodes Based on a Cobalt Tetraazamacrocyclic Catalyst. *ACS Catal.* **2021**, *11* (6), 3662–3678. <https://doi.org/10.1021/acscatal.0c05033>.
- (39) Nie, C.; Liu, C.; Gong, L.; Wang, M. Boosting the Performance of a Silicon Photocathode for Photoelectrochemical Hydrogen Production by Immobilization of a Cobalt Tetraazamacrocyclic Catalyst. *J. Mater. Chem. A* **2021**, *9* (1), 234–238. <https://doi.org/10.1039/D0TA09942B>.
- (40) Schnorr, J. M.; Swager, T. M. Emerging Applications of Carbon Nanotubes. *Chem. Mater.* **2011**, *23* (3), 646–657. <https://doi.org/10.1021/cm102406h>.
- (41) De Volder, M. F. L.; Tawfick, S. H.; Baughman, R. H.; Hart, A. J. Carbon Nanotubes: Present and Future Commercial Applications. *Science* **2013**, *339* (6119), 535–539. <https://doi.org/10.1126/science.1222453>.
- (42) Karousis, N.; Tagmatarchis, N.; Tasis, D. Current Progress on the Chemical Modification of Carbon Nanotubes. *Chem. Rev.* **2010**, *110* (9), 5366–5397. <https://doi.org/10.1021/cr100018g>.
- (43) Li, X.; Lei, H.; Guo, X.; Zhao, X.; Ding, S.; Gao, X.; Zhang, W.; Cao, R. Graphene-Supported Pyrene-Modified Cobalt Corrole with Axial Triphenylphosphine for Enhanced Hydrogen Evolution in PH 0-14 Aqueous Solutions. *ChemSusChem* **2017**, *10* (22), 4632–4641. <https://doi.org/10.1002/cssc.201701196>.

- (44) Reuillard, B.; Warnan, J.; Leung, J. J.; Wakerley, D. W.; Reisner, E. A Poly(Cobaloxime)/Carbon Nanotube Electrode: Freestanding Buckypaper with Polymer-Enhanced H₂-Evolution Performance. *Angew. Chem. Int. Ed.* **2016**, *55* (12), 3952–3957. <https://doi.org/10.1002/anie.201511378>.
- (45) Zamader, A.; Reuillard, B.; Pécaut, J.; Billon, L.; Bousquet, A.; Berggren, G.; Artero, V. Non-Covalent Integration of a [FeFe]-Hydrogenase Mimic to Multiwalled Carbon Nanotubes for Electrocatalytic Hydrogen Evolution. *Chem. Eur. J.* **2022**. <https://doi.org/10.1002/chem.202202260>.
- (46) Tran, P. D.; Le Goff, A.; Heidkamp, J.; Jusselme, B.; Guillet, N.; Palacin, S.; Dau, H.; Fontecave, M.; Artero, V. Noncovalent Modification of Carbon Nanotubes with Pyrene-Functionalized Nickel Complexes: Carbon Monoxide Tolerant Catalysts for Hydrogen Evolution and Uptake. *Angew. Chem. Int. Ed.* **2011**, *50* (6), 1371–1374. <https://doi.org/10.1002/anie.201005427>.
- (47) Maurin, A.; Robert, M. Noncovalent Immobilization of a Molecular Iron-Based Electrocatalyst on Carbon Electrodes for Selective, Efficient CO₂-to-CO Conversion in Water. *J. Am. Chem. Soc.* **2016**, *138* (8), 2492–2495. <https://doi.org/10.1021/jacs.5b12652>.
- (48) Reuillard, B.; Ly, K. H.; Rosser, T. E.; Kuehnel, M. F.; Zebger, I.; Reisner, E. Tuning Product Selectivity for Aqueous CO₂ Reduction with a Mn(Bipyridine)-Pyrene Catalyst Immobilized on a Carbon Nanotube Electrode. *J. Am. Chem. Soc.* **2017**, *139* (41), 14425–14435. <https://doi.org/10.1021/jacs.7b06269>.
- (49) Pugliese, S.; Huan, N. T.; Forte, J.; Grammatico, D.; Zanna, S.; Su, B.; Li, Y.; Fontecave, M. Functionalization of Carbon Nanotubes with Nickel Cyclam for the Electrochemical Reduction of CO₂. *ChemSusChem* **2020**, cssc.202002092. <https://doi.org/10.1002/cssc.202002092>.
- (50) Li, F.; Zhang, B.; Li, X.; Jiang, Y.; Chen, L.; Li, Y.; Sun, L. Highly Efficient Oxidation of Water by a Molecular Catalyst Immobilized on Carbon Nanotubes. *Angew. Chem. Int. Ed.* **2011**, *50* (51), 12276–12279. <https://doi.org/10.1002/anie.201105044>.
- (51) Creus, J.; Matheu, R.; Peñafiel, I.; Moonshiram, D.; Blondeau, P.; Benet-Buchholz, J.; García-Antón, J.; Sala, X.; Godard, C.; Llobet, A. A Million Turnover Molecular Anode for Catalytic Water Oxidation. *Angew. Chem. Int. Ed.* **2016**, *55* (49), 15382–15386. <https://doi.org/10.1002/anie.201609167>.
- (52) Rajabi, S.; Ebrahimi, F.; Lole, G.; Odrobina, J.; Dechert, S.; Jooss, C.; Meyer, F. Water Oxidizing Diruthenium Electrocatalysts Immobilized on Carbon Nanotubes: Effects of the Number and Positioning of Pyrene Anchors. *ACS Catal.* **2020**, *10* (18), 10614–10626. <https://doi.org/10.1021/acscatal.0c01577>.
- (53) Gimbert-Suriñach, C.; Albero, J.; Stoll, T.; Fortage, J.; Collomb, M.-N.; Deronzier, A.; Palomares, E.; Llobet, A. Efficient and Limiting Reactions in Aqueous Light-Induced Hydrogen Evolution Systems Using Molecular Catalysts and Quantum Dots. *J. Am. Chem. Soc.* **2014**, *136* (21), 7655–7661. <https://doi.org/10.1021/ja501489h>.
- (54) Laviron, E. General Expression of the Linear Potential Sweep Voltammogram in the Case of Diffusionless Electrochemical Systems. *Journal of Electroanalytical Chemistry and Interfacial Electrochemistry* **1979**, *101* (1), 19–28. [https://doi.org/10.1016/S0022-0728\(79\)80075-3](https://doi.org/10.1016/S0022-0728(79)80075-3).
- (55) Bajada, M. A.; Roy, S.; Warnan, J.; Abdiaziz, K.; Wagner, A.; Roessler, M. M.; Reisner, E. A Precious-Metal-Free Hybrid Electrolyzer for Alcohol Oxidation Coupled to CO₂-to-

- Syngas Conversion. *Angewandte Chemie* **2020**, *132* (36), 15763–15771. <https://doi.org/10.1002/ange.202002680>.
- (56) Muckerman, J. T.; Fujita, E. Theoretical Studies of the Mechanism of Catalytic Hydrogen Production by a Cobaloxime. *Chem. Commun.* **2011**, *47* (46), 12456. <https://doi.org/10.1039/c1cc15330g>.
- (57) Sun, D.; Karippara Harshan, A.; Pécaut, J.; Hammes-Schiffer, S.; Costentin, C.; Artero, V. Hydrogen Evolution Mediated by Cobalt Diimine-Dioxime Complexes: Insights into the Role of the Ligand Acid/Base Functionalities. *ChemElectroChem* **2021**, *8* (14), 2671–2679. <https://doi.org/10.1002/celec.202100413>.
- (58) Reuillard, B.; Costentin, C.; Artero, V. Deciphering Reversible Homogeneous Catalysis of the Electrochemical H₂ Evolution and Oxidation: Role of Proton Relays and Local Concentration Effects. *Angew. Chem. Int. Ed.* **2023**, *62* (36), e202302779. <https://doi.org/10.1002/anie.202302779>.
- (59) Amtawong, J.; Montgomery, C. L.; Bein, G. P.; Raithel, A. L.; Hamann, T. W.; Chen, C.-H.; Dempsey, J. L. Mechanism-Guided Kinetic Analysis of Electrocatalytic Proton Reduction Mediated by a Cobalt Catalyst Bearing a Pendant Basic Site. *J. Am. Chem. Soc.* **2024**, *146* (6), 3742–3754. <https://doi.org/10.1021/jacs.3c10408>.
- (60) Costentin, C.; Savéant, J.-M. Multielectron, Multistep Molecular Catalysis of Electrochemical Reactions: Benchmarking of Homogeneous Catalysts. *ChemElectroChem* **2014**, *1* (7), 1226–1236. <https://doi.org/10.1002/celec.201300263>.
- (61) Velasco, L.; Liu, C.; Zhang, X.; Grau, S.; Gil-Sepulcre, M.; Gimbert-Suriñach, C.; Picón, A.; Llobet, A.; DeBeer, S.; Moonshiram, D. Mapping the Ultrafast Mechanistic Pathways of Co Photocatalysts in Pure Water through Time-Resolved X-Ray Spectroscopy. *ChemSusChem* **2023**, *16* (21), e202300719. <https://doi.org/10.1002/cssc.202300719>.
- (62) Kaminsky, C. J.; Weng, S.; Wright, J.; Surendranath, Y. Adsorbed Cobalt Porphyrins Act like Metal Surfaces in Electrocatalysis. *Nat. Catal.* **2022**, *5* (5), 430–442. <https://doi.org/10.1038/s41929-022-00791-6>.
- (63) Hutchison, P.; Kaminsky, C. J.; Surendranath, Y.; Hammes-Schiffer, S. Concerted Proton-Coupled Electron Transfer to a Graphite Adsorbed Metalloporphyrin Occurs by Band to Bond Electron Redistribution. *ACS Cent. Sci.* **2023**, *9* (5), 927–936. <https://doi.org/10.1021/acscentsci.3c00186>.
- (64) Costentin, C.; Savéant, J.-M. Homogeneous Molecular Catalysis of Electrochemical Reactions: Manipulating Intrinsic and Operational Factors for Catalyst Improvement. *J. Am. Chem. Soc.* **2018**, *140* (48), 16669–16675. <https://doi.org/10.1021/jacs.8b09154>.
- (65) Simándi, L. I.; Szeverényi, Z.; Budó-Záhonyi, É. Activation of Molecular Hydrogen by Cobaloxime(II) Derivatives. *Inorg. Nucl. Chem. Letters* **1975**, *11* (11), 773–777. [https://doi.org/10.1016/0020-1650\(75\)80098-5](https://doi.org/10.1016/0020-1650(75)80098-5).
- (66) Simándi, L. I.; Budó-Záhonyi, É.; Szeverényi, Z. Effect of Strong Base on the Activation of Molecular Hydrogen by Pyridinebis(Dimethylglyoximato)Cobalt(II). *Inorg. Nucl. Chem. Letters* **1976**, *12* (3), 237–241. [https://doi.org/10.1016/0020-1650\(76\)80158-4](https://doi.org/10.1016/0020-1650(76)80158-4).
- (67) Shinagawa, T.; Takanabe, K. Towards Versatile and Sustainable Hydrogen Production through Electrocatalytic Water Splitting: Electrolyte Engineering. *ChemSusChem* **2017**, *10* (7), 1318–1336. <https://doi.org/10.1002/cssc.201601583>.
- (68) Segev, G.; Kibsgaard, J.; Hahn, C.; Xu, Z. J.; Cheng, W.-H. (Sophia); Deutsch, T. G.; Xiang, C.; Zhang, J. Z.; Hammarström, L.; Nocera, D. G.; Weber, A. Z.; Agbo, P.; Hisatomi, T.; Osterloh, F. E.; Domen, K.; Abdi, F. F.; Haussener, S.; Miller, D. J.; Ardo, S.; McIntyre, P.

C.; Hannappel, T.; Hu, S.; Atwater, H.; Gregoire, J. M.; Ertem, M. Z.; Sharp, I. D.; Choi, K.-S.; Lee, J. S.; Ishitani, O.; Ager, J. W.; Prabhakar, R. R.; Bell, A. T.; Boettcher, S. W.; Vincent, K.; Takanabe, K.; Artero, V.; Napier, R.; Cuenya, B. R.; Koper, M. T. M.; Van De Krol, R.; Houle, F. The 2022 Solar Fuels Roadmap. *J. Phys. D: Appl. Phys.* **2022**, *55* (32), 323003. <https://doi.org/10.1088/1361-6463/ac6f97>.